Journal of Advances in Mechanical Engineering and Science, Vol. 4(1) 2018, pp. 45-54

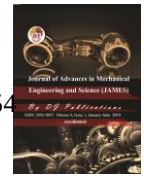

RESEARCH ARTICLE

Effect of Graphite Coating on Microstructure and Corrosion Properties of High Power Diode Laser Surface Melting of 7075 Aluminum Alloy

[*]A.C Umamaheshwer Rao[1], V Vasu[2], K.V Sai Srinadh[2]

[1]Department of Mechanical Engineering Sreyas Institute of Engineering and Technology, Hyderabad, India.

[2]Department of Mechanical Engineering, National Institute of Technology Warangal, Telangana, India.

Received- 24 January 2018, Revised- 1 May 2018, Accepted- 18 May 2018, Published- 22 May 2018

ABSTRACT

In this article, a high power diode laser is used for surface melting a 7075-T651 aluminum alloy with and without graphite coating to induce microstructural changes on the surface and to improve corrosion resistance. LSM (Laser Surface Melting) is investigated using 3 kW power with the scan rate of 4 mm/s and 5 mm/s for the graphite coated and non-coated samples in the nitrogen atmosphere respectively. The microstructural analysis observations show that, most of the grain boundaries of the wrought structure and the coarse constituent phase are altered in the re-solidified laser melted layer. The potentiodynamic polarization of the alloy is determined using corrosion study, whereas the electrochemical impedance study is evaluated by treating the alloy in 3.5% sodium chloride solution. Based on this study, it is observed that the corrosion current of the laser treated sample is reduced by 5 times when compared to the un-treated samples. Superior corrosion resistance occurs due to the absence of coursed constituent phases at the surface of the laser-melted layer.

Keywords: High power diode laser, Graphite coating, Corrosion, Potentiodynamic polarization, Electrochemical impedance.

1. INTRODUCTION

7075 aluminum alloys exhibit high strength to weight ratio and possess better mechanical properties due to precipitate hardening process. It finds use in structural and aerospace sectors due to its high strength and eminent properties. It is prone to pitting and stress corrosion cracking when interacting with the corrosion environments. The main alloying elements of the 7075 Al alloy are Mg, Cu, Zn, Fe and traces of other intermetallic elements such as Ti, Cr, Si and Mn. Al alloy [1] comprises two types of constituent particles to contribute high strength and corrosion behavior, which includes (i) particles like Al, Mg and Zn that are anodic with regard to the matrix and promptly dissolve (ii) particles such as Fe, Cu and Mn behave as cathodic to the matrix and incline that promote dissolution of the adjoining matrix. As a result of formation of constituent particles, galvanic impact occurs, thus developing corrosion pits at the particle interface. These constituent particles form intermetallic phases such as Mg_2Si, $(Al, Cu)_6$ (Fe, Cu) and Al_7Cu_2Fe, in which the Al_7Cu_2Fe is reported to be the foremost cathodic part, which ends within the development of pitting corrosion at the particle- matrix interface [2]. For this series of Al alloys, numerous heat treatments process are available to minimize the corrosion rates. The over aging process is one among the heat treatments, which provide resistance to hydrogen transportation along the grain boundaries by developing a course precipitates and aggregate structure along it. Lamentably,

*Corresponding author. Tel.:+919885696023
Email address: umamaheswar.ac@sreyas.ac.in (A.C.U.Rao)
Double blind peer review under responsibility of DJ Publications
https://dx.doi.org/10.18831/james.in/2018011005

as contrast to T6 temper, the strength of Al alloy is lessened by 10 to 15%. LSM, a non-traditional technique of surface engineering has the ability to overcome the above drawbacks up to sure extent and conjointly provide profound interest to enhance the corrosion resistance of aluminium alloys. This technique has the capacity to vary the surface properties of the alloy without changing its bulk properties.

LSM provides rapid melting of the surface and has fast solidification that result in a homogeneous and fine surface, which are exempted from unwanted intermetallic particles. After the completion of short irradiation, LSM leads to fast quenching of the liquefied material into the cold subsurface through the conduction process [3]. Consequently, LSM creates a thin liquefied layer of alloy surface with a resulting high level of homogenization and refinement of the microstructure in the close surface, that locales through disintegration and redistribution of inclusion or precipitates and phase transformations [4-6]. Several researches are done to investigate the laser treatment of Al alloy surface. [7] has studied the Stress corrosion cracking behavior of Nd:YAG laser-treated aluminum alloy 7075, in which LSM is done using nitrogen and air. When treated with N_2 atmosphere that acts a electrical insulator, an enhancement in corrosion resistance owing to the formation of fine cellular/dendritic structures with evacuation of coarse constituent particles is determined and an AIN phase is detected.

[8] has studied the effect of LSM on Stress Corrosion Cracking (SCC) behavior of 6013 Aluminum alloy in 3.5% NaCl and reported that SCC resistance is increased due to the formation of non-dendrite layer, and it is free from coarse constituents phases in the re-solidified layer. Also, it is observed that LSM results in an oxide-nitride phase at the top surface, which acts as a barrier against the cracks. [7] has investigated–the laser-treated surface using a KrF excimer laser on 7075 aluminum alloy, and it is found that the laser-treated layer consists of 5-6 nm polycrystalline α-Al_2O_3 with some undetermined precipitates. The vicinity of chemically stable nano-crystalline structures α-Al_2O_3 at the surface, serves as a viable boundary to secure the matrix against corrosion. [9] has investigated the microstructure and mechanical properties of Al 5052 using equal channel angular pressing method to improve hardness and tensile property.

Many researches have been done using CO_2, EXCIMER and Nd-YAG lasers sources with small beam spot radius. A problem of overlapping adjacent tracks results at lasing large surface area, which ultimately increases the cost and process time. The overlap zone is also subjected to further heat treatment that ends in microstructural variations. Due to its high sensitivity to inhomogeneties, corrosion resistance degrades. Process cost and degradation in corrosion resistance are minimized using a High Power Diode Lasers (HPDLs) with large laser spot where HPLD comprises larger surface coverage and desired melt depth with low overlapping [10]. This work intends to pertinence HPDL's in corrosion and characterization studies before and after laser treatment. Also most of the work is done on the bare alloy without any light absorbing coatings. Al has poor capacity of absorbing light. The aluminium alloy surface is suitably prepared by surface treatment or deposition of a suitable absorbent prior to laser re-melting. In this laser surface re-melting of 7075 alloy, graphite (Gr) is used as an absorbent, which has an absorbtion coefficient in the range of 60 to 80% [11, 12]. The effect of graphite coating before laser treatment on the microstructure and corrosion behavior is investigated.

2. EXPERIMENTATION

AA7075-T6, a wrought aluminum alloy that belongs to Al-Zn-Mg-Cu family is used as a base material. Table 1 presents the chemical composition of the alloy. Peak aged Al alloy in the form of plate with thickness of 6.35 mm is considered. The sample surface is initially polished with Silicon Carbide (SiC) grit paper prior to graphite coating. A colloidal graphite (60-80 µ graphite powder) is painted on its surface (approximately 0.2 mm), and then laser treatment is carried out by employing continuous wave high power (3 kW) fiber-coupled diode laser at 4 mm/s transverse speed. Laser treatment is also performed on the bare material without graphite coating as shown in table 2. This laser has emission wavelength of 890-980 nm and laser spot size of 20 mm X 5 mm. Surface

treatment is done on a working distance of 300 mm in the presence of N_2 shroud gas at 2 bar pressure from off-axial shroud nozzle. Laser treatment is done along the transverse direction of the plate that is perpendicular to the rolling direction.

Table 1.Chemical composition (w %) of 7075-T6 aluminum alloy

Zn	Mg	Cu	Fe	Si	Cr	Mn	Ti	other	Al
5.5	2.4	1.3	0.16	0.05	0.223	0.03	0.07	0.15	bal

Electrochemical measurement is conducted using a conventional three-electrode system in 3.5% NaCl solution purged with N_2 gas. A 10 mm X 10 mm exposed area, Saturated Calomel Electrode (SCE) and platinum (Pt) electrode is utilized as the working electrode, reference electrode and counter electrode respectively. Electrochemical interface SI1287 combined with impedance/gain phase analyser SI1260 from solartron is used to perform the potentiodynamic polarization and impedance test with an initial delay time of 30 min, polarization scan rate of –1.5 to –0.5 V and frequency of 100000 to 0.1 Hz.

Table 2.Summary of laser parameters used for laser processing

Laser power	3 kW
Liner speed	5 mm/s with Gr coat 4 mm/s without Gr coat
Size of focused laser spot	20 mm X 5 mm
Working distance	300 mm
Laser energy density	80-160 J/mm^2
Shrouding gas	N_2 at 2 bar

The microstructural analysis and phase composition of the surface are characterized using light microscopy, in which Keller's enchant reagent is used to etch the Al alloy. Hardness test is experimented on equidistant spaced cross sectioned samples using micro hardness machine with a load of 50 grams and dwell time of 10 s. Scanning Electron Microscope (SEM) (Test Scan, Czech Republic) equipped with Energy Dispersive Spectrometry (EDS) is used to analyse the microstructure and X-ray diffraction model. Panalytical, X'Pert PRO model is employed to study the phases present before and after LSM.

3. RESULTS AND DISCUSSIONS

3.1. Microstructure analysis

The unprocessed alloy consists of different constituent phases such as CuAl2, $MgZn_2$, AlSi and Al_7Cu_2Fe and also some Si containing phases running along the rolling direction. The presence of these phases is reported in [2]. Figure 1 shows the stereographic cross sectional image of laser surface melted Al 7075 alloy treated with graphite coating. The laser treatment is employed with an applied energy density of 150 J/mm^2 and 120 J/mm^2 for the bare metal and graphite coated sample respectively. It is observed that the microstructure consists of melted zone, interface and the heat affected zone without any defects on its surface.

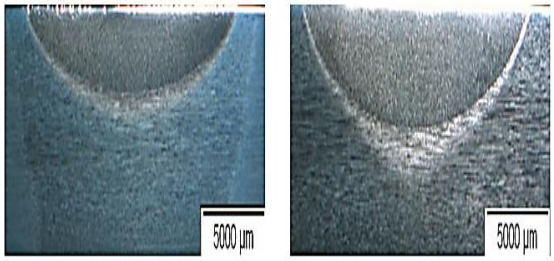

Figure 1.Low magnification cross sectional stereographic image LSM samples lassed with (a) 150 J/mm^2 (b) 120 J/mm^2 with Gr coating

The laser melted zone comprises a depth of 3.2 mm and 2 mm with an interface thickness of 700 µm and 200 µm for samples with and without graphite coating respectively. Carbon coating enhances the heat absorption thereby increases the depth of the melted sample whereas in graphite coating, the width of the processed zone is less than the focused laser beam (20 mm), which are attributed to the laser intensity distribution. The laser depth and width are summarised in table A1. The cross sectional microstructure of various zones of laser treated surface is shown in figure 2. It is observed that the planar growth occurs at the base of modified layer as seen in figure B1 (c), whereas the remaining layer comprises segregated cellular structure, and the microstructure at the surface of the laser melted region is observed to be fine and dendrite as shown in figure B1 (a). Hardness test is carried out across the melt depth of the LSM samples, and it is observed that the sample treated with Gr coating results in high

hardness than the normal LSM. The hardness plots are shown in figure 2. The microstructure of alloy contains different intermetallic particles (primary particles), which are not dissolved or left outside during the solubilisation treatment. Apart from primary particles, sub-micrometer particles are also observed due to the secondary hardening precipitates of the artificial ageing process.

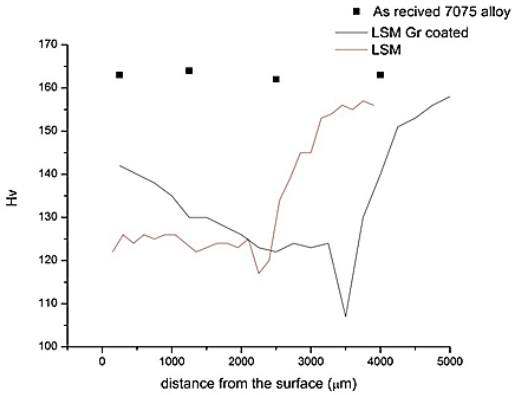

Figure 2.Hardness profile across the cross-section of the untreated and laser treated sample

In Al alloy, an iron source arises from the impurities during the alloy production that tends to the development of constituent particles. These constituent particles are irregularly shaped and relatively large with dimension ranging from few tenths of a micron up to 10 micro meters and classified as large sized particles in the alloy. These particles usually nucleate during alloy solidification and are not appreciably dissolved while subsequent thermo-mechanical processing. On the other hand, mechanical treatments like extrusion and rolling tend to disintegrate and align these constituent particles in bands within the alloy. As these particles are rich in alloying elements, their electrochemical behavior is often different from the surrounding matrix phase due to galvanic effect thus resulting in corrosion.

Figure B2 shows the SEM images related to the surface of the treated and untreated laser samples at high magnification. A numerous large sized coarse constituent phases and precipitates are present in the alloy. The identification of the constituent particles has been done through SEM compositional mapping and SEM- EDS analysis as shown in figure 3. From the SEM-EDS analysis, it is observed that these phases are rich in iron, copper and magnesium. After LSM, fine structure of about 2-4 microns are dispersed uniformly throughout the surface as seen in figures B2 (b) and (c). These dispersed phases are formed at dendritic boundaries in discontinuous networks due to non-equilibrium solidification of the molten metal. The solidification of the last supersaturated liquid in alloy elements at the grain boundaries tends to form agglomerates in large numbers.

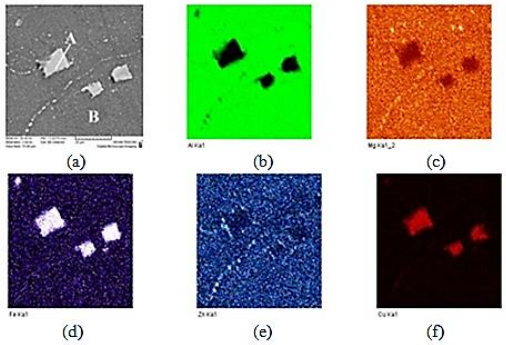

Figure 3.SEM-EDX mapping analysis of AA 7075-T6 alloy (a) Micrograph of the surface revealing the presence of dispersed phase (b) Al (c) Mg (d) Fe (e) Zn (f) Cu

EDS analysis shown in table A2 consolidates the weight % elements analysis of the untreated and laser treated samples on the phases and the matrix respectively. From EDS analysis, it is observed that the dispersed phase consists of Cu, Mg and Zn elements. It is also observed that the composition of the alloying elements such as Fe and Cu are drastically decreased after LSM. The fine and uniform distribution of dispersed phases after LSM is also observed from the EDS compositional mapping as in figure 4.

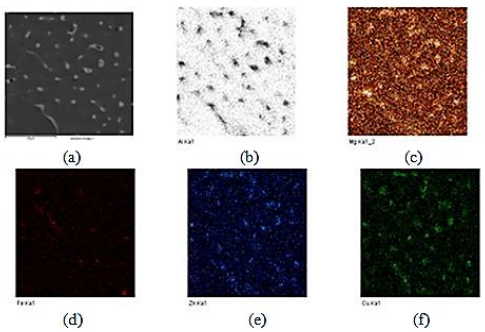

Figure 4.SEM-EDX mapping analysis of LSM of Gr coated sample (a) Micrograph of the surface revealing the presence of dispersed phase (b) Al (c) Mg (d) Fe (e) Zn (f) Cu

The elimination of such large constituent particles at the grain boundary and within the grain of the unprocessed alloy improves the resistance to corrosion, and delays the formation of SCC [13].

3.2. X-ray diffraction

The results of low angle X-ray diffraction of the AA 7075-T6 alloy before and after LSM with various heat inputs are showed in figures 5 and 6. It can be seen that alloys consists of large number of second phase particles such as $MgZn_2$, Al_7Cu_2Fe, $CuAl_2$ and Mg_2Si. These particles have major contribution towards the corrosion initiation, especially AlCuFe. After laser treatment, no significant high peaks are observed in second phases.

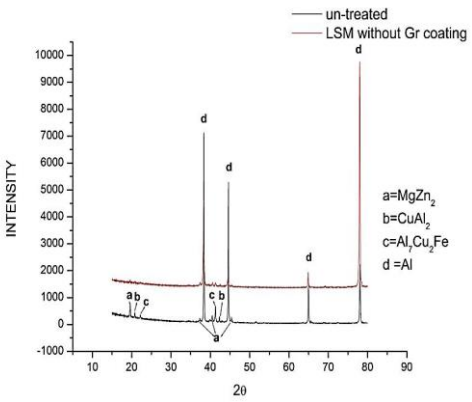

Figure 5.XRD of untreated and laser treated sample

A high intensity of peak is observed in the low angle X-ray diffraction of the graphite coated sample due to the presence of carbon in laser melted region as depicted in figure 6. The constituent intermetallic phases such as Mg_2Si, AlCuMg and Al_7Cu_2Fe are absent [14].

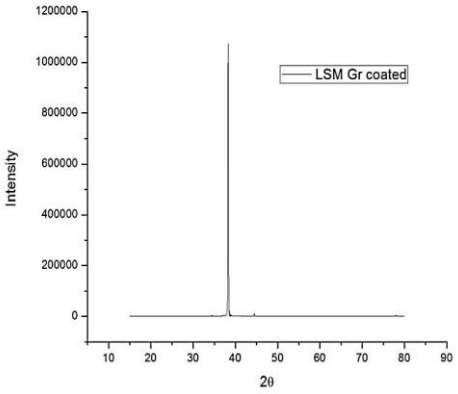

Figure 6.XRD of LSM with Gr coating

3.3. Corrosion analysis

3.3.1. Potentiodynamic polarization test

Potentiodynamic polarization curves for the unprocessed AA 7075-T6 alloy and laser-treated specimen in deaerated 3.5% NaCl solution are shown in figure 7.

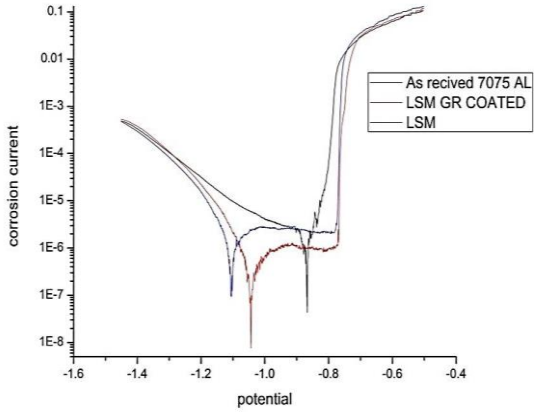

Figure 7.Potentiodynamic polarization curves of untreated and laser treated sample

The curves reveal that there is a reduction by 2 and 6 orders of magnitude in the corrosion current (I_{corr}) for LSM and LSM with Gr coating specimens respectively when compared with the unprocessed alloy. The corrosion current density is decreased from 3.4 $X10^{-6}$ A/cm^2 to $7.2X10^{-7}$ A/cm^2 in case of Gr coating specimens whereas in case of laser melted surface, significant passive film formation is observed. Furthermore, repassivation potential is observed below that of E_{corr} (corrosion potential), suggesting the favorable growth of corrosion pits in the immersed corrosive solution. No significant passive film formation could be noticed in the potentiodynamic plot of untreated alloy indicating easy progression of corrosion. It is well known that presence of constituent particles such as Al-Cu-Fe and $AlCu_2$ etc. can easily promote galvanic effects across their boundaries and thereby leads to the formation of nucleate corrosion pits. As laser melting substantially reduces these constituent particulates, promotion of corrosion attack at the particle-to-grain boundary leading to pit formation gets substantially reduced. Similar studies conducted with different laser treated conditions also report the vast reduction in corrosion currents of melted layers produced with precipitate-free surface. The potentiodynamic curve of laser melted surface

shows a longer region of passivity spanning 0.2 - 0.25 V range indicating the vast reduction in anodic current and enhancement of pitting corrosion resistance. Indeed the presence of high amount of such phases in untreated surface increases the cathodic activity and thus enhances corrosion attack [15]. The decrease in current attributes to the reduction of the corrosion rate due to alteration in size, shape and composition of the second phase of the untreated sample. Decreasing current may also be considered due to the absence of coarse second phase particles on the surface as a result of homogeneous surface formation on the laser treated sample, which further allows to develop continuous passivation film resulting in overall better corrosion resistance. Corrosion rates of untreated and laser treated samples are given in table A3.

3.3.2. Electrochemical impedance

The impedance measurements of the Electrochemical Impedance Spectroscopy (EIS) experiment are displayed as Nyquist plots. The results obtained for the untreated and laser-treated specimens at Open Circuit Potential (OCP) are shown in figure 8. EIS plots suggest the well-defined and poorly-defined loop in high and low-frequency range.

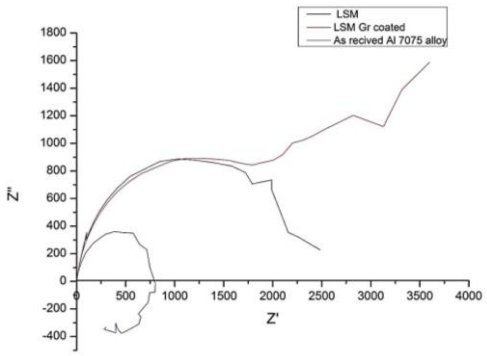

Figure 8.Nyquist plots of untreated and laser treated samples

The loops (semicircles) represent film impedance at various stages constituting high and low-frequency electron transfer reaction. The plots suggest similar pitting corrosion behavior in both laser-melted and untreated conditions but with distinguishably varied degrees. It is well known that corrosion proceeds with corroded surface film formation at the site of defects and progresses with film build-up. Based on the resistance of the film and its disintegration, its corrosion resistance is determined. It is clear from the loop contours that laser melted surface with and without graphite coating shows remarkable enhancement in corrosion resistance when compared to untreated substrate. Apart from the laser treated sample, the graphite coated sample shows more improvement in corrosion resistance as seen in figure 8.

To interpret the electrochemical behavior of the EIS spectra, equivalent circuits comprising resistance and capacitance elements are constructed and depicted in figure 9, where the calculated values are appended in table A4. Rp, a sum of both film resistance and charge transfer resistance (R_{coat} + R_{corr}) increases in three –fold and eight fold for laser melted sample with and without graphite coating respectively when compared to untreated specimen. The results obtained are in concurrence with previously obtained potentiodynamic polarization test. For the untreated specimen, due to significant amounts of coarse constituent particles and discontinuous film formation, the initial oxide film may not provide adequate protection and the particles themselves can promote localized corrosion attacks. For the laser melted specimen, the elimination of coarse primary constituent particles definitely inhibits localized corrosion and improves the continuity of the film. As a result, film resistance increases and thereby imparting good corrosion resistance.

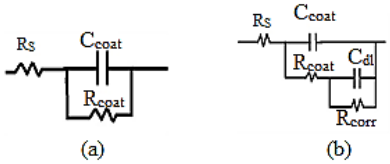

Figure 9.Equivalent circuits for insertion reactions (a) untreated material, (b) laser treated samples

In figure 9, R_S is the electrolyte resistance, R_{coat} refers to the film resistance, R_{corr} is the charge-transfer resistance, C_{coat} denotes the film capacitance and C_{dl} is the double-layer capacitance.

4. CONCLUSION

Laser surface treatment of large area without over lapping of laser tracks has significantly improved the corrosion resistance of 7075 alloy. Further, addition of graphite coating prior to laser melting, results in improvement of corrosion resistance due to enhanced heat absorption, thus resulting in

more homogenization at the sample surface. The improvement in corrosion resistance of the alloy is due to the reduction of constituent particles in the laser modified layer as well as the chemical homogenization of the matrix material. The re-solidified laser-melted layer is refined by altering the shape, size and composition of detrimental constituent particles and the grain boundary network present in wrought structure. From SEM-EDS analysis after LSM, it is observed that fine structure (about 2-3 microns) is dispersed uniformly throughout the surface that are rich in Cu and Mg. XRD results indicate that after LSM, the major constituent particles such as Mg_2Si, $CuAl_2$ and Al_7Cu_2Fe are absent. The comparative corrosion study determined by Potentiodynamic Polarization measurements in 3.5% sodium chloride solution shows that the corrosion current is reduced by 6 times in laser melted surface compared to un-treated substrate. The corrosion rate is drastically decreased after LSM. It shows that LSM has a profound effect the corrosion.

REFERENCES

[1] M.Gao, C.R.Feng and R.P.Wei, An Analytical Electron Microscopy Study of Constituent Particles in Commercial 7075-T6 and 2024-T3 Alloys, Metallurgical and Materials Transaction A, Vol. 29, No, 4, 1998, pp. 1145-1151, https://dx.doi.org/10.1007/s11661-998-0240-9.

[2] N.Birbilis, M.K.Cavanaugh and R.G.Buchheit, Electrochemical Behavior and Localized Corrosion Associated with Al_7Cu_2Fe Particles in Aluminum Alloy 7075-T651, Corrosion Science, Vol. 48, No. 12, 2006, pp. 4202-4215, https://dx.doi.org/10.1016/j.corsci.2006.02.007.

[3] S.J.Kalita, Microstructure and Corrosion Properties of Diode Laser Melted Friction Stir Weld of Aluminum Alloy 2024 T351, Applied Surface Science, Vol. 257, No. 9, 2011, pp. 3985-3997, https://dx.doi.org/10.1016/j.apsusc.2010.11.163.

[4] K.G.Watkins, M.A.Mcmahon and W.M.Steen, Microstructure and Corrosion Properties of Laser Surface Processed Aluminium Alloys: A Review, Materials Science and Engineering: A, Vol. 231, No. 1-2, 1997, pp. 55-61, https://dx.doi.org/10.1016/S0921-5093(97)00034-8.

[5] X.Y.Wang, Z.Liu and P.H.Chong, Effect of Overlaps on Phase Composition and Crystalline Orientation of Laser-Melted Surfaces of 321 Austenitic Stainless Steel, Thin Solid Films, Vol. 453, 2004, pp. 72-75, https://dx.doi.org/10.1016/j.tsf.2003.11.078.

[6] Z.Liu, P.H.Chong, P.Skeldon, P.A.Hilton, J.T.Pencer and B.Quayle, Fundamental Understanding of the Corrosion Performance of the Laser Melted Metallic Alloys, Surface Coatings Technology, Vol. 200, No. 18-19, 2006, pp. 5514–5525, https://dx.doi.org/10.1016/j.surfcoat.2005.07.108.

[7] T.M.Yue, L.J.Yan and C.P.Chan, Stress Corrosion Cracking Behavior of Nd: YAG Laser-Treated Aluminum Alloy 7075, Applied Surface Science, Vol. 252, No. 14, 2006, pp. 5026-5034, https://dx.doi.org/10.1016/j.apsusc.2005.07.052.

[8] W.L.Xu, T.M.Yue and H.C.Man, Stress Corrosion Cracking Behaviour of Excimer Laser Treated Aluminium Alloy 6013, Materials Transactions, Vol. 49, No. 8, 2008, pp. 1836-1843, https://dx.doi.org/10.2320/matertrans.MRA2008105.

[9] N.Nandakumar and V.Ranjithkumar, Experimental Investigation of Microstructure and Mechanical Properties of Al 5052 Processed by Equal Channel Angular Pressing Technique, Journal of Advances in Mechanical Engineering and Science, Vol. 4, No. 1, 2018, pp. 38-44, https://dx.doi.org/10.18831/james.in/2018011004.

[10] T.M.Yue, L.J.Yan, C.P.Chan, C.F.Dong, H.C.Man and G.K.H.Pang, Excimer Laser Surface Treatment of Aluminum Alloy AA7075 to improve Corrosion Resistance, Surface and

Coatings Technology, Vol. 179, No. 2-3, 2004, pp. 158-164, https://dx.doi.org/10.1016/S0257-8972(03)00850-8.

[11] T.Kek and J.Grum, Influence of the Graphite Absorber during Laser Surface Hardening, Journal of Mechanical Engineering, Vol. 56, No. 2, 2010, pp. 150-157.

[12] R.Sturm, J.Grum and S.Bozic, Influence of the Alloying Elements in Al-Si Alloys on the Laser Remelting Process, Lasers in Engineering, Vol. 22, No. 1-2, 2012, pp. 47- 61.

[13] C.P.Chan, T.M.Yue and H.C.Man, The Effect of Excimer Laser Surface Treatment on the Pitting Corrosion Fatigue Behaviour of Aluminium Alloy 7075, Journal of Materials Science, Vol. 38, No. 12, 2003, pp. 2689-2702, https://dx.doi.org/10.1023/A:1024498922104.

[14] A.U.Rao, V.Vasu, S.M.Shariff and K.S.Srinadh, Influence of Diode Laser Surface Melting on Microstructure and Corrosion Resistance of 7075 Aluminium Alloy, International Journal of Microstructure and Materials Properties, Vol. 11, No. 1-2, 2016, pp. 85-104, https://dx.doi.org/10.1504/IJMMP.2016.078055.

[15] A.Benedetti, M.Cabeza, G.Castro, I.Feijoo, R.Mosquera and P.Merino, Surface Modification of 7075-T6 Aluminium Alloy by Laser Melting, Surface and Interface Analysis, Vol. 44, No. 8, 2012, pp. 977-981, https://dx.doi.org/10.1002/sia.4840.

APPENDIX A

Table A1.Laser nomenclature and laser energy densities

Nomenclature	Laser energy density J/mm^2	Depth of melt (mm)	Width of melt (mm)	Surface hardness (Hv)
A	150	2	17.3	120-115
B	120 with Gr coating	3.2	18.8	145-140

Table A2.EDS spot spectrum analysis on the untreated and laser treated samples

Sl. No	Elements wt%	Spot A	Spot B	Spot C	Spot D	Spot E	Spot F	Spot G
1	Mg	0.26	5.47	2.90	5.40	1.60	8.59	2.33
2	Al	55.68	70.86	87.69	76.33	93.23	63.7	90.49
3	Fe	12.60	0.02	0.14	0.07	0.03	0.07	0.09
4	Cu	29.57	5.32	1.68	5.59	0.48	10.00	0.85
5	Zn	1.65	18.21	7.43	12.42	4.42	17.39	6.23

Table A3.Corrosion rates of untreated and laser treated samples

Sample ID	Corrosion rate (mpy)	Io (A/cm^2)	Eo (Volts)
Untreated alloy	1.5	3.42E-06	-0.87
150J/mm^2	0.92	2.09E-076	-1.10
120J/mm^2 with Gr coated	0.31	7.23E-07	-1.04

Table A4.Calculated values for the various equivalent circuit elements at OCP

Sl. No	Energy density (J/mm^2)	R_s	C_{coat}	R_{coat}	C_{dl}	R_{corr}	R_p
1	Untreated alloy	0.95		0	3.37E-05	789.3	789.3
2	150 J/mm^2	2.016	2.88E-05	1868	0.00032	548	2416
3	120 J/mm^2 with Gr coating	1.858	2.11E-05	1878	0.00054	4644	6522

APPENDIX B

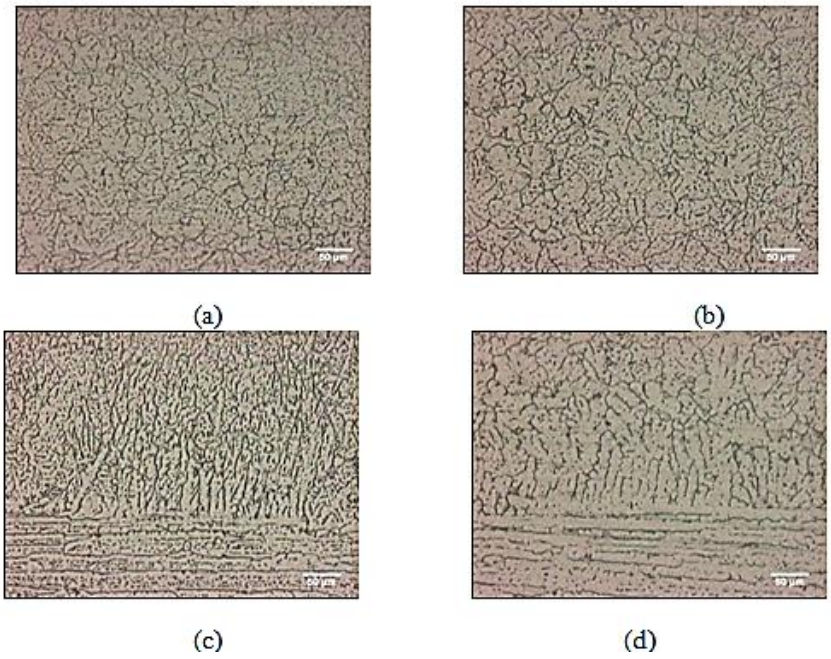

Figure B1.Microstructure of laser treated surface (a) near the top of laser treated surface without coating (b) near the top of laser treated surface with Gr coating, (c) and (d) are the fusion zone without and with laser coatings respectively

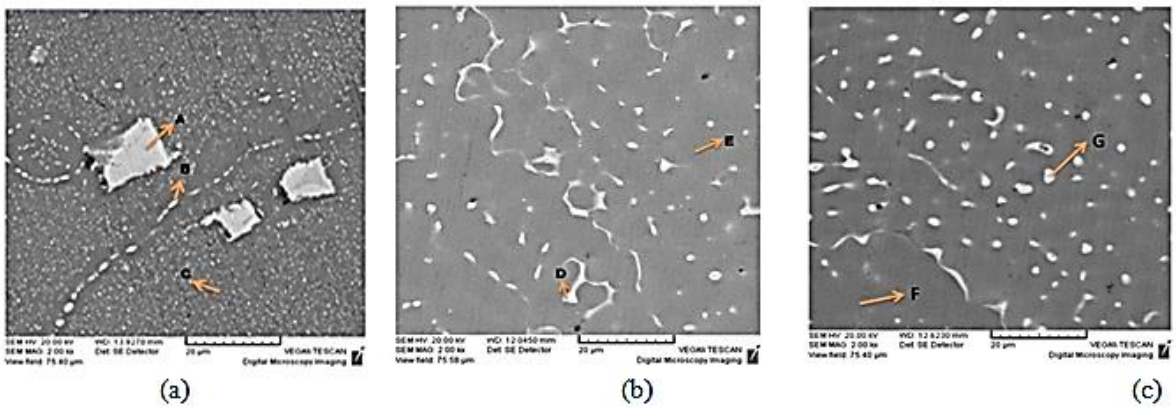

Figure B2.EDS spot spectrum analysis on surface of the samples (a) Untreated 7075 Al alloy (b) Sample lased with 150/mm^2 (c) Sample lased with 120J/mm^2 with Gr coating.